On neutronographic texture analysis

K.Feldmann and L. Fuentes. Joint Institute for Nuclear Research, Laboratory for Neutron Physics

RESUMEN

Se revisan aspectos básicos del análisis de texturas. Se presentan los conceptos fundamentales asociados a la función de distribución de orientaciones en agregados policristalinos sobre la base del método de desarrollo en series. Se describen los métodos de determinación de texturas mediante difractometría neutrónica y se comparan entre sí las técnicas de dispersión angular y tiempo de vuelo. Se exponen resultados experimentales representativos correspondientes a diversos sistemas. Se discute la relación entre la textura y las propiedades policristalinas. Se introducen las tendencias actuales del análisis de texturas, incluidas las llamadas "texturas fantasmas" y la simulacion por computadoras de la formación de texturas durante la deformación plástica.

ABSTRACT

A review is given of some basic aspects of texture analysis. The main concepts related to the orientation distribution function of polycrystalline solids are presented on the basis of the series expansion method. Neutron diffraction techniques for texture determination are described and a comparison between "classical" angle-dispersive and time-of-flight methods is carried out. Representative experimental results are given for several different systems. The relation between texture and polycrystal properties is discussed. Present trends in texture analysis are considered, including the so-called "ghost-phenomena" and the computer simulation of texture formation as a result of plastic deformation process.

INTRODUCTION

Many of single crystal properties such as Young's modulus, hardness, magnetic susceptibility etc. are anisotropic. Therefore, the average of these physical properties in technically important polycrystalline materials depends on the frequency of crystallites in the various orientations, the so-called texture of the material which is completely described by the orientation distribution function (ODF), to be defined below. Hence, physical properties of investigated specimen can be calculated, if its ODF is known. Many technologically important processes like plastic deformation, crystallization, phase transitions, etc. may vary crystallite orientations. Therefore, changes of preferred crystalline orientations may be used as a sensitive indicator giving insight into such processes. These are strong reasons why the knowledge of the ODF of polycrystalline materials is important for materials science and metallurgical industries as well as for progress in understanding of microscopic moving and ordering processes in solids, for example, in solid state deformation theories. Furthermore, the final texture can be used as an indicator for the history of the material. This latter aspect is especially relevant in geology where it provides information about processes which have taken place millions years ago.

At present, widely used methods to investigate the texture of a given sample are pole figure determination by x-ray or thermal neutron diffraction. The corresponding ODF is obtained by computer analysis of the information contained in several pole figures.

TEXTURE DESCRIPTIONS AND MEASUREMENT:

The most straightforward, but very time consuming approach to determine the ODF starts from single orientation measurements obtained most from electron diffraction or optical birefringence /1,2/. An alternative method allowing for a high statistical relevance and high angular resolving power, is an integrating measurement of all crystallites with a given orientation in the specimen. Techniques of this type are pole figure determinations by X-ray or thermal neutron diffraction.

A pole figure is a presentation, on a stereographic projection of the distribution of a particular crystallographic direction with respect to the specimen geometry. In Fig. 1a the stereographic projection of the points P and Q on the unit sphere to P and Q on the equator plane is shown. Rotating the sample with respect to the scattering vector all the sphere can be covered with experimental points. In this manner the intensity distribution of the Bragg reflection (hkl) in dependence on sample position

is determined. The specimen rotations are realized by means of a special texture goniometer consisting in general of three independent rotational axes being perpendicular to each other like it is schematically shown in Fig. 2. Fig.1b represents the experimental pole figure (0002) from a rolled Ti-sheet. The specimen geometry is specified by the three orthogonal directions: RD (rolling direction). TD (transverse direction) and ND (surface normal direction) in the centre of pole figure. Because of the symmetry of this pole figure it is sufficient to measure one quadrant of the stereographic projection to represent the texture.

The orientation of a crystallite in the sample is described by the three angular parameters. Two angles fix a given crystallographic direction (hkl) with respect to the specimen coordinate system. The crystal can be rotated around this direction to be described by the third angular parameter which is "lost" in pole figure measurements. Therefore, the threedimensional ODF has to be computed on the base of several pole figures of different crystallographic directions. The mathematical background for this treatment is given in a later section.

An alternative method for presenting texture information is the inverse pole figure. The importance of this technique increases especially with progress in texture investigation by means of energy dispersive X-ray and neutron time-of-flight diffraction. The inverse pole figure is a presentation on a stereographic projection of the distribution of a particular specimen direction with respect to the crystal geometry. In Fig.3 the irreductible inverse pole figure ranges are shown for cubic and hexagonal crystal lattices. They are specified by (001), (101) and (111) directions in the cubic and by (0001), (1010) as well as (1120) directions in the hexagonal case. In analogy to normal pole figures the inverse pole figure is represented by two orientation parameters as well. The third one is lost because of the possible rotation of the sample around the given sample direction.

At present widest used method for texture analysis is the angle dispersive X-ray diffraction. Because of the two or three orders lower linear absorption coefficients of neutrons in the most of materials both angle dispersive and time-of-flight neutron diffraction are more powerfull tools, specially for volume texture determination. There are two serious difficulties raising from high absorption of X-rays in materials:

- The measurement of outer pole figure range which can be determined in transmission scattering geometry only. In the case of high specimen and crystallographic symmetries an inversion of incomplete pole figures can be used to obtain the ODF. The expense for this treatment increases rapidly with decreasing symmetries of sample and crystal lattice.

- Usually, X-ray texture investigations are limited to fine grained materials being a serious restriction for geological problems especially.

The important restraint of neutron texture analysis consists in its coupling to an efficient neutron source, i.e. to a nuclear reactor.

The following discussions are restricted to neutron methods only. The basic equation for any diffraction technique, Bragg's law:

$$\lambda = 2\, d_{hkl} \sin \Theta \qquad (1)$$

contains two variables for a given Bragg reflection (fixed d_{hkl}), i.e. neutron wave length λ and Bragg angle Θ. One of them is kept constantly in the experiment. Respectively, are two methods for neutron diffraction:

- In the stationary angle dispersive method a monochromatic neutron beam is used. The neutron flux which hits the sample is constant during the experiment. To analyze various Bragg reflections (different d_{hkl}) the angle Θ is changed.
- Using the full neutron spectrum which contains all wave lengths λ, the complete diffraction pattern can be detected at constant scattering angle 2Θ. In this so-called time-of-flight (TOF) method the neutron wave length (or energy) $\lambda \sim E^{-\frac{1}{2}}$) is determined via time of flight of the recorded neutron for a known flight parh L. The linear relation

$$\lambda[\mathrm{nm}] = 396.78\ T\ [\mathrm{s}]/L\ [\mathrm{m}] \qquad (2)$$

connects the wave length λ with time of flight T. For TOF method the neutron beam has to be pulsed. This technique is similar to the energy dispersive X-ray diffraction /3,4/. In Fig.4 the Bragg law is shown in a λ-Θ coordinate system for a bcc crystal. Lines being parallel to the λ-axis (Θ=const.) correspond to a TOF experiment; parallel to the Θ-axis (λ=const) the angle dispersive method is characterized. The intersection with the curves for different lattice planes determine the position of Bragg reflections in the diffraction pattern. Furthermore Fig.4 shows the TOF method to be able to record all non-forbidden reflection contrary to angle dispersive technique. For texture analysis by means of angle dispersive method double axis diffractometers are used. The integrated intensities of one Bragg reflection (hkl) are determined in dependence on specimen position with respect to the scattering angle successively. The aperture and the collimation in front of the detector are choosen in a manner to tecord the complete peak intensity in one diffractometer position. In this case one pole figure is determined, given by discrete network of points. A number of pole figures has to be measured for several independent Bragg reflections to get unambiguous results concerning the texture of investigated specimen.

In TOF technique an experimental equipment is used like shown schematically in Fig.5. Pole figures can be measured in the same way as in angle dispersive method determining Bragg reflections in dependence on a sample position with respect to the scattering vector $\vec{H}$. Contrary to the angle dispersive method, in all measurable pole figures the equipositioned points are determined in one experiment simultaneously. On the other hand the simultaneous recording of all reflections corresponds to that information which is necessary for inverse pole figure composition. Therefore the TOF technique is a straightforward method to determine inverse pole figures. The integral intensities of Bragg reflections, i.e. peak areas, of TOF diffraction spectra are computed by means of fit programs. Such a procedure enables to use the information of overlapping peaks for texture analysis contrary to angle dispersive method where separated reflexes are considered only. Fig.6 illustrates the situation for overlapped reflections showing texture effects.

If data handling via inverse pole figures is possible, the texture formation in dependence on external influences (temperature, pressure, fields) can be observed in TOF experiments immediately because of its fixed scattering geometry. Equivalent investigations by conventional technique would be much more expansive.

In this way the opening of the neutron TOF diffraction for texture analysis gives the possibility to investigate a much wider spectrum of problem in this fields. On the other hand, the expanse for data handling and measurement time is approximately independent of the number of determined pole figures, but much higher than for angle dispersive studies of samples having cubic or hexagonal lattice symmetry. Therefore, the TOF method should be used especially for problems requiring a large number of pole figures for mathematical texture analysis, i.e. for low symmetry and multiphased substances. A second field for TOF technique are in situ investigations of texture formation processes.

MATHEMATICAL BACK GROUD

The orientation of the crystal coordinate system fixed at given cell with respect to the sample system attached to the specimen can be described by Eulerian angles α, β, γ, represented by g (see Fig.7) /5/.

The orientation distribution of the crystallites in the sample is then quantitatively characterized by the ODF f(g)

$$\int_G f(g)\,dg = 1, \quad dg = \sin\beta\, d\alpha\, d\beta\, d\gamma/8\pi^2 \qquad (3)$$

with

$$G : 0 \leq \alpha, \ \gamma \leq 2\pi, \ 0 \leq \beta \leq \pi$$

Assuming that all crystallites possess the same shape and size, then f(g) is the probability density for a crystallite in the sample to have the orientation g.

The symmetry properties of the considered crystal are reflected in the ODF, i.e.

$$f(g) = f(g.g_\mu) \tag{4}$$

where g_μ represents any rotation of the point group of the crystal. In many cases the sample possesses any symmetry, which is not mathematically exact, like rotational symmetry in wires or orthorhombic symmetry in rolled sheets. This means, equivalently to equ. 4 the condition holds

$$f(g) = f(g_\nu.g) \tag{5}$$

for specimen symmetries. The equs. 1 and 2 limit the irreducible range of ODF to be determined for complete texture analysis.

How to reproduce ODF from experimental pole figures or inverse pole figures? This problem is discussed by Matthies /5-13/ in general form. Up to now some methods are known for pole figure inversion to calculate ODF from experimental results, for example the so called vector method proposed by Ruer and Baro /14-15/ and the Imhof-method /16, 17/. Widely used is a treatment basing on series expansion of ODF and pole figures which is proposed by Roe and Bunge /19, 20/. In the following this method is outlined in a compact form. The ODF can be expanded into a series of generalized spherical harmonics

$$f(g) = \sum_{\ell=0}^{\infty} \sum_{m=-\ell}^{\ell} \sum_{n=-\ell}^{\ell} C_\ell^{mn} T_\ell^{mn}(g) \tag{6}$$

On the other hand pole figures are specific twodimensional projections of the threedimensional ODF. In this way the pole figure $\vec{h}_i = [hkl]$ can be expanded into a series of spherical harmonics with the same coefficients C_ℓ^{mn} which are used in equ. 4.

$$P_{\vec{h}_i}(\vec{y}) = \sum_{\ell=0}^{\infty} \sum_{m=-\ell}^{\ell} \sum_{n=-\ell}^{\ell} \frac{4\pi}{2\ell+1} C_\ell^{mn} k_\ell^m(\vec{h}_i) k_\ell^n(\vec{y}) \tag{7}$$

The unit vector $\vec{y}$ gives the direction in the specimen coordinate system. If there are symmetries of the crystal lattice and the sample some of C_1^{mn} vanish identically. Therefore, Bunge has introduced linear combinations of spherical harmonics

$$T_\ell^{\mu\nu}(g) = \sum_{m=-\ell}^{\ell} \sum_{n=-\ell}^{\ell} (A_\ell^{m\mu})^* A_\ell^{n\nu} T_\ell^{mn}(g) \tag{8}$$

and

$$k_\ell^\mu(\vec{h}) = \sum_{m=-\ell}^{\ell} A_\ell^{m\mu} k_\ell^m(\vec{h}) \tag{9}$$

$$k_\ell^\nu(\vec{y}) = \sum_{m=-\ell}^{\ell} A_\ell^{n\nu}\, k_\ell^n(\vec{y})$$

respectively. The coefficients $A_\ell^{m\mu}$ and $A_\ell^{n\nu}$ are chosen in a way that spherical harmonics reflect crystal symmetry (index μ) and specimen symmetry (ν) /20/. For a given crystal symmetry and series expansion degree there are M(1) linearly independent possibilities to construct symmetrical harmonics $k_\ell^\mu(\vec{h})$. For sample symmetry there are N(1) variants of $k_\ell^\nu(\vec{y})$ respectively. In Fig.8 M(!) is shown for different symmetries and even ℓ only. Unfortunately in general diffraction experiments are not able to distinguish reflexions h and -h because of Friedel's law. Therefore, only mixed pole figures

$$\tilde{P}_{h_i}(y) = \frac{1}{2N_{h_i}} [P_{h_i}(y) + P_{-h_i}(y)] \qquad (10)$$

can be measured. Taking into account the condition

$$k_\ell^\mu(h_i) = (-1)^\ell k_\ell^\mu(-h_i) \qquad (11)$$

as well as equ.7, the formula for the experimental pole figure $\vec{h}_i$ has to be written as follows:

$$\tilde{P}_{\vec{h}_i}(\vec{y}) = \frac{4\pi}{N_{\vec{h}_i}} \sum_{\ell=0}^{\infty} \sum_{\mu=1}^{M(\ell)} \sum_{\nu=1}^{N(\ell)} \frac{(1+(-1)^\ell)}{2(2\ell+1)}\, C_\ell^{\mu\nu}\, k_\ell^{\mu\nu}(\vec{h}_i)\, k_\ell^\nu(\vec{y}) \qquad (12)$$

where N_{h_i} is the pole figure normalization factor. If ℓ is odd, the corresponding term on the right side of equation 12 vanishes. This is no reason $C_\ell^{\mu\nu}$ for odd ℓ to be zero, but it is impossible to calculate them from diffraction experiments. In this way, a reduced ODF f(g) composed from even ℓ $C_\ell^{\mu\nu}$ can be determined only. The true ODF has the form

$$f(g) = \tilde{f}(g) + \tilde{\tilde{f}}(g), \qquad (13)$$

where $\tilde{\tilde{f}}(g)$ describes the odd ℓ part. This mentioned loss of information leads to the so - called ghost effects in reduced ODFs. Conceptions for their corrections will be discussed later. Equation 10 connects experimental pole figures with a reduced ODF via series expansion coefficients for even ℓ only

$$\tilde{f}(g) = \sum_{\ell=0(2)}^{\infty} \sum_{\mu=1}^{M(\ell)} \sum_{\nu=1}^{N(\ell)} C_\ell^{\mu\nu}\, T_\ell^{\mu\nu}(g) \qquad (14)$$

To simplify $C_\ell^{\mu\nu}$ determination the orthonormality of spherical harmonics can be used if complete pole figures are available. Multiplying equation 10 with $k_\ell^{\nu*}(\vec{y})$ and integrating about the full pole figure range

$$F_\ell^\nu(\vec{h}_i) = \frac{4\pi}{N_{\vec{h}_i}} \oint \tilde{P}_{\vec{h}_i}(\vec{y})\, k_\ell^{\nu*}(\vec{y})\, d\vec{y} \qquad (15)$$

a factor $F_\ell^\nu(h_i)$ is calculated, which is connected with series expansion coefficients by

$$F_\ell^\nu(\vec{h_i}) = \sum_{\mu=1}^{M(\ell)} \frac{4\pi}{2\ell+1} C_\ell^{\mu\nu} k_\ell^\mu (\vec{h_i}) \qquad (16)$$

This equation system is of low order compared with equ.10. Usually the number of measured pole figures should be greater than $M(\ell_{max})$ to minimize the influence of experimental errors by means of a least square fit.

Finally, the normalization factor of pole figure is given by

$$N_{\vec{h_i}} = \oint \tilde{P}_{\vec{h_i}}(\vec{y})\, \vec{d_y} \qquad (17)$$

If pole figures are described by polar coordinates the increment $\vec{dy}$ is equal to $\sin\beta d\beta d\alpha$ where α is the azimuth. The adequate way to calculate series coefficients from inverse pole figures is not important up to now. Furthermore, the series expansion formalism includes the possibility to compute $C_\ell^{\mu\nu}$ from incomplete pole figures. This is important especially for the X-ray texture analysis having serious difficulties to measure the pole figure range near the equator. In detail the incomplete pole figure treatment is outlined in /21,22/.

RESULTS

The most prominent symmetry contribution for which quantitative texture investigation have been carried out is cubic crystal symmetry connected with sheet symmetry assumed as mmm. As an example Fig. 9a shows pole figures measured by means of angle dispersive neutron diffraction. The specimen was the eutectic alloy Al - 5% Ca - 5% Zn (% = weight per cent). The sample was reduced with a degree of 87% by hot rolling at 550°C with 75% by cold rolling. After that the specimen was superplastically deformed at 550°C with strain rate $1.2\ 10^{-1}$ to a degree of 50 per cents. From the experimental pole figures, the ODF was calculated. It is shown in Fig. 9b.

At the IBR-30 reactor of JINR, Dubna, a rolled sheet of microduplex steel has been studied. The specimen consists of α and γ phase of iron with bcc and fcc lattice respectively. On 30m flight path diffraction patterns have been measured for different sample positions at constant scattering angle $2\theta = 90°$ /23,24/. Fig. 10 shows the important part of TOF spectra for specimen orientations ND, RD and TD. The texture effect leads to relative intensity changes for different reflections from one spectrum to the other. With the help of a fit program, 7 peaks for each phase could be separated, i.e. 14 pole figures could be determined simultaneously. Texture analysis, including data from the angle dispersive method /25,26/

has given interesting results, concerning interactions between texture components of both phases.

It was mentioned above, that the information of one TOF diffraction pattern is equivalent to the corresponding inverse pole figure. This fact has been used to observe texture formation during recrystallization process of copper immediately /27/. The sample was composed from 96% deformed copper bars possessing axial specimen symmetry. In this case the inverse pole figure of symmetric axis contains the full texture information. Because of the low neutron flux at IBR-30 reactor, the minimum time for one TOF spectrum is about 2 hours. Therefore, a constant temperature of 225°C has been chosen to extend the recrystallization process up to 35 h. In Fig.11 the TOF spectra before and after heating are compared with the diffraction pattern of texture free copper powder. Measurements have been carried out in intervals of 2 h. Fig.12 shows inverse pole figures for different recrystallization times measured at the stationary reactor RFR of CINR Rosendorf. The deformation texture of copper bars consists of two components <100> and <111>. Relative intensity changes of (111) and (100) points refer to texture modifications during recrystallization process. The integral intensity of (111), (200), (311) and (422) reflections depending on heating time is represented in Fig.13. It is shown that a large number of grains passes from orientation (111) to the (100) one. Very powerfull pulsed neutron sources like the new IBR-2 reactor of the JINR, Dubna, will allow more realistic studies of recrystallization. The technologically interesting processes of this kind turn out in less 1 hour.

Using the neutron TOF diffraction for the texture analysis, there are interesting perspectives for investigation of geological problems. A lot of minerals have low lattice symmetry. Therefore, their fabric structure cannot de investigated by means of angle dispersive techniques efficiently At the IBR-30 reactor the quartz phase texture of a granulite sample has been studied. Quartz has trigonal lattice symmetry. In this case the (hkil) and (khil) reflections cannot be separated in any diffraction pattern although they are not structurally equivalent. Nevertheless, the full quantitative texture analysis can be carried out if any pole figure with h = k and 1 = 0 has been determined. From TOF spectra of granulite, 8 pole figures could be separated. They are shown in Fig.14. Fig.15 represents the ODF computed from experimental data.

TEXTURE AND PROPERTIES

Now the relation between texture and physical properties in a polycrystalline sample is briefly discussed. Let us represent the relation between two orientation dependent quantities X and Y by the physical property E having r-rank tensor character:

$$Y = E \cdot X. \tag{18}$$

Here Y is a measurable m - rank tensor, X is a measurable n - rank tensor, and m + n = r. Examples of properties described by fourth-rank tensors are the compliance and its inverse, the stiffness, while the refraction index and the electrical conductivity are second-rank tensors.

In the Hill approximation, neglecting the orientation correlation among crystallites, the polycrystal mean value of a property is given by the simple averaged quantity $\bar{E}$ determined by:

$$\bar{E} = \frac{1}{v} \int E(\vec{r})\, dv \tag{19}$$

This in turn may be calculated using as a weight function the ODF:

$$\bar{E} = \int E(g)\, f(g)\, dg \tag{20}$$

Here the integration domain is the Euler space.

If the property under consideration is an orientation dependent scalar, for example the Young modulus or the magnetization energy in a magnetic field, then equation (3) simplifies to

$$\bar{E}(y) = \oint E(\vec{h}) R_{\vec{y}}(\vec{h})\, d\Omega \tag{21}$$

where $R_{\vec{y}}(\vec{h})$ is the inverse pole figure for the sample direction $\vec{y}$. The integration is taken over the projection sphere.

In equation (20) the texture is characterized by the complete ODF. There is an alternative averaging method that employs only the low-order expansion coefficients $C_{\ell}^{\mu\nu}$ of the ODF. It can be shown that the components of the polycrystalline averaged property E are given by:

$$\bar{E}_{i_1 \ldots i_r} = \sum_{j_1 j_2 \ldots j_r} \bar{a}(i_1 i_2 \ldots i_r ; j_1 j_2 \ldots j_r)\, E_{j_1 j_2 \ldots j_r} \tag{22}$$

where

$$\bar{a}(i_1 \ldots i_r ; j_1 \ldots j_r) = \sum_{\ell=0}^{r} \sum_{\mu} \sum_{\nu} \bar{a}_{\ell}^{\mu\nu}(i_1 \ldots i_r ; j_1 \ldots j_r) C_{\ell}^{\mu\nu} \tag{23}$$

Here $E_{j_1 \ldots j_r}$ are the components of the monocrystal tensor. The averaging coefficients $\bar{a}(i_1 \ldots i_r ; j_1 \ldots j_r)$ characterize the texture, as they depend on $C_{\ell}^{\mu\nu}$. It should be noted that only the coefficients up to $l = r$ (rank of E) enter in the average equations. The geometrical factors $\bar{a}_{\ell}^{\mu\nu}(i_1 \ldots j_r)$ are general quantities for a given crystal and sample symmetry. They are tabulated in /28/.

The method of equation (21) could be driven to a useful coefficient form as well. Tensors are partially (but comprehensibly) characterized in the so-called surface representation by an orientational dependent scalar. This is the case, for example, of the elastic tensor and the Young modulus (see, Nye /29/. For second-rank tensors the surface representation is given by the scalar $E(\vec{h}) = \vec{h}\cdot\overleftrightarrow{E}\cdot\vec{h}$, described by the ellipsoid

$$E = E_{11}h_1^2 + E_{22}h_2^2 + E_{33}h_3^2 \tag{24}$$

where E_{ii} (i = 1,2,3) are the components of $\overleftrightarrow{E}$ in the principal axis coordinate system and h_i are the projections of the unit vector $\vec{h}$ on axis i. For cubic crystals, all E_{ii} are equal, and thus, second-rank properties are isotropic.

Expanding the monocrystal property E(h) in the symmetric harmonics:

$$E(\vec{h}) = \sum_{\ell=0}^{r} \sum_{\mu} e_\ell^\mu \, k_\ell^\mu \, (\vec{h}) \tag{25}$$

and averaging, it follows that

$$\bar{E}(\vec{y}) = \sum_{\ell} \sum_{\nu} \bar{e}_\ell^\nu \, k_\ell^\nu \, (\vec{y}) \tag{26}$$

for the texturized polycrystal. Here the averaging coefficients are given by

$$\bar{e}_\ell^\nu = \frac{1}{2\ell+1} \sum_{\mu} e_\ell^\mu \, C_\ell^{\mu\nu} \tag{27}$$

So, the knowledge of the monocrystal parameters e_ℓ^μ and those of the texture coefficients $C_1^{\mu\nu}$(1=0,...,r) permits to determine the averaged polycrystal property $\bar{E}(\vec{y})$.

For the so-called uniaxial properties, like the Young modulus, all the odd-ℓ parameters e_ℓ^μ are zero. In these cases, the considered polycrystal property is independent of the odd part of the ODF.

PRESENT TRENDS IN TEXTURE ANALYSIS

At present one of the most puzzling problems in texture analysis is the loss of information of the ODF, determined from pole figure measurements, i.e. the problem of so-called ghost phenomena, being able to falsify the ODF markedly.

"Ghosts" were firstly characterized by Matthies /30/. This author has systematically investigated their properties and searched for practical methods to determine them /5-13/.

In the following, some methods to correct or to elude ghost effects are discussed briefly.

Wagner et al. /31/ have avoided diffraction based measurements of po

le figures. They applied a polarizing microscope method to determine the orientation of individual grains in samples of birefringent substances like calcite. For the considered class of materials their result appear promissing, notwithstanding the tediousness of the experimental procedure. Bunge and Esling /32, 38/ propose to determine the odd part of the ODF using zero - domains of pole figures. These zero -domains must imply ranges g_F in the unreduced ODF, where f(g) is identical to zero as well. Then the equation holds:

$$\tilde{f}(g_F) = -\tilde{\tilde{f}}(g_F) \qquad (28)$$

From this condition the $C_\ell^{\mu\nu}$ coefficients for 1 odd can be calculated. Of course, such a treatment is restricted to sharp textures with true zero-domains in pole figures.

Another analytical method permitting the correction of ghost phenomena is the representation of the ODF by model components (most Gaussians) /34/. The fit is not too complicated if the ODF consists of a few sharply separated components only. For overlapping peaks a number of secondary conditions must be taken into account. This method avoids all series truncation errors arising in the Bunge-Roe method.

In /35/ the experimental possibilities have been evaluated tc measure unreduce pole figures using anomalous scattering of X-rays or neutrons respectively. In quartz-like structures the principal possibility of low degree ghost corrections is demonstrated, supposing high experimental accuracy. According to /35/ the use of anomalous neutron scattering to determine odd part of the ODF is possible for selected elements only.

For a number of typical orientation of cubic materials, maps of f(g) have been computed for a normalized Gaussian in the Euler space /12, 36/. Comparing these maps with reduced ODFs, calculated from experimental pole figures, ghost phenomena could be excluded in a high degree.

Finally, Matthies et al. /12, 37, 38/ have proposed a new method to reproduce the ODF from pole figures using a so-called conditional ghost correction. The method is an iterative procedure, basing partly on consideration of Williams /39/ and Imhof /17/ as well as on the condition $f^n(g) \geq 0$. The number of required iteration steps is influenced by the choice of zero approximation sufficiently.

A further problem of high importance in texture research is the study of prefered orientation formation as a result of a plastic deformation process by computer simulation. The model, introduced by taylor in 1938 /40/ gives the conceptional basis of this theory. According to this conception, the preferred orientation arises from the reorientation of the crystallites if they undergo intragranular deformation associated with

the glide motion of dislocations. Fig.16 presents the physical idea of the Taylor model. In a given mechanical treatment on the sample, the shown crystallite is obliged to deform from (a) to (b). From the energetical point of view the deformation has not only to consist of simple gliding, but must be connected with a rotation of crystal axes as well.

Taylor demonstrated that any given homogeneous crystal deformation could be represented by different superposition of no more than 5 contributions of glide deformations and axes rotations, and has introduced the calculation of the work needed for all such superpositions. In his model the actual path of the crystallite is that, associated with the minimum necessary work (Principle of Minimum Work). To predict the orientation distribution in a deformed polycrystal, the Taylor method prescribes the analysis on each crystallite of the optimum (minimum work) superposition of deformations and rotations driving the crystallite to the same macroscopic deformation as the whole sample.

Experimentally measured textures of metals are well near from those calculated with the Taylor model. The theory has been further developed, so permitting the consideration of more complicated systems and other deformation mechanisms. Important works in this direction are those of Bishop and Hill /41, 42/ on the mathematical formulation of the problem and of the yielding condition, the planning by Chin and Mammel /43/ of the problem as a dual linear programming task and the simulation by Lister, Patterson and Hobbs /44/ of texture formation on low-symmetry systems (quartz rocks).

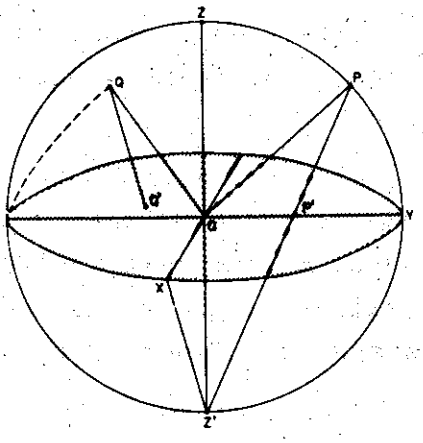

Figure 1a

Stereographic projection of the points P and Q from the unit sphere to P' and Q' on the equator plane.

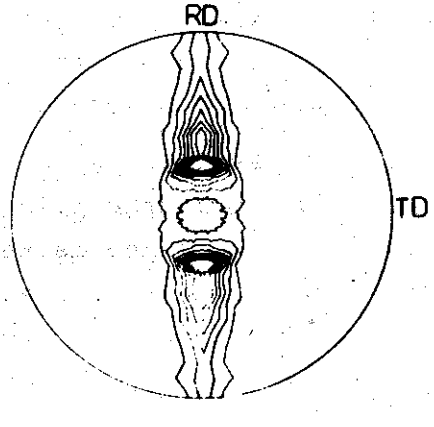

Figure 1b

Distribution density of (hkl) lattice plane normals of all crystallites in the stereographic projection (pole figure).

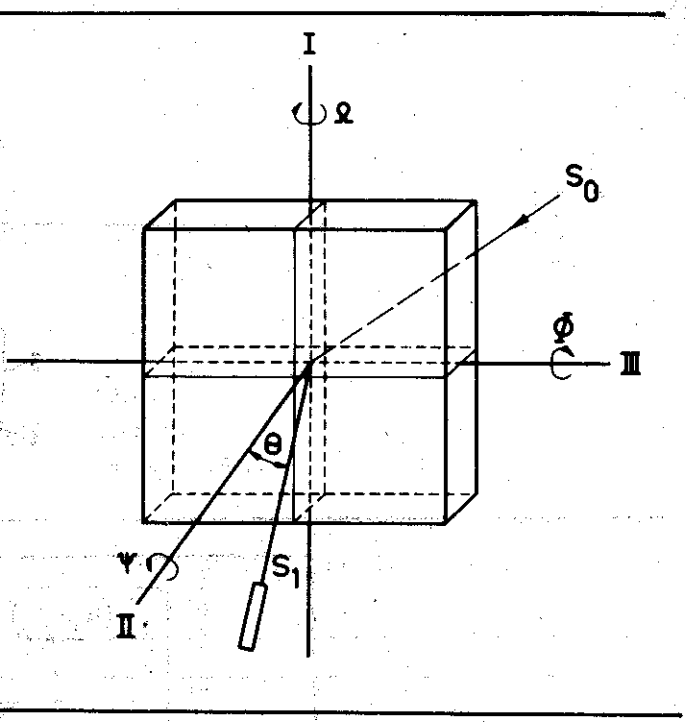

Figure 2

Scheme of a texture goniometer. 1-primary beam. 2-detector, Ω, Φ, Ψ -rotation axes.

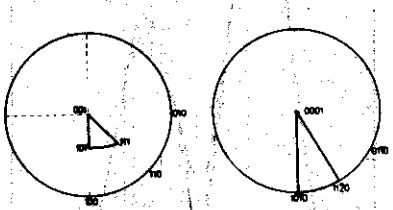

Figure 3

Irreducible ranges of inverse pole figures for cubic and hexagonal lattices.

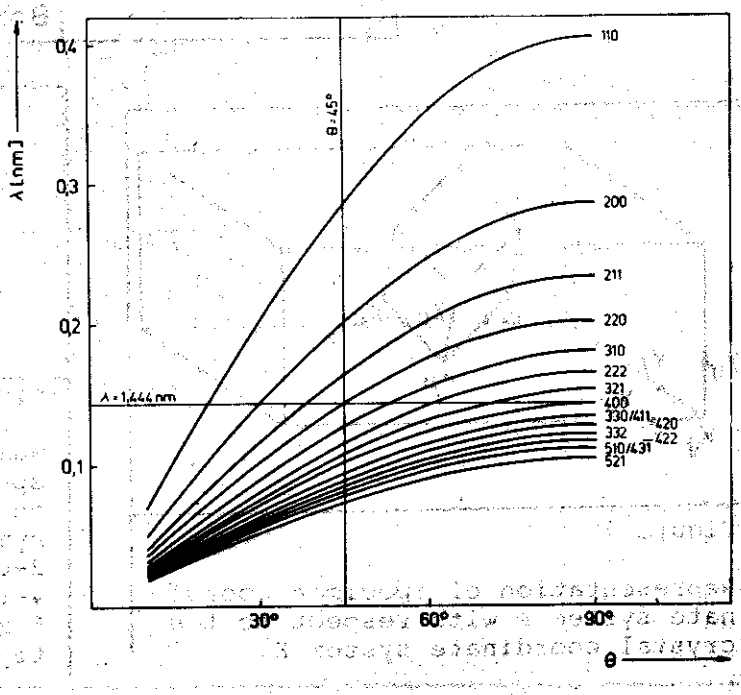

Figure 4

Representation of Bragg's law in a θ - λ - coordinate system. The curves correspond to reflections from a bcc lattice.

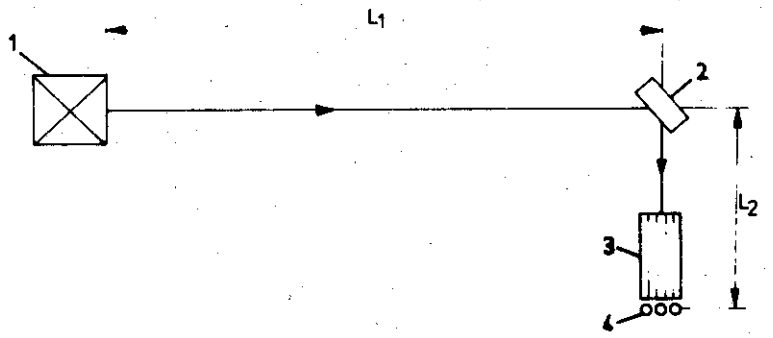

Figure 5

Scheme of a TOF texture spectrometer. 1-neutron source, 2-specimen with texture goniometer, 3-slit collimator, 4-detector, L_1,L_2-first and second flight path.

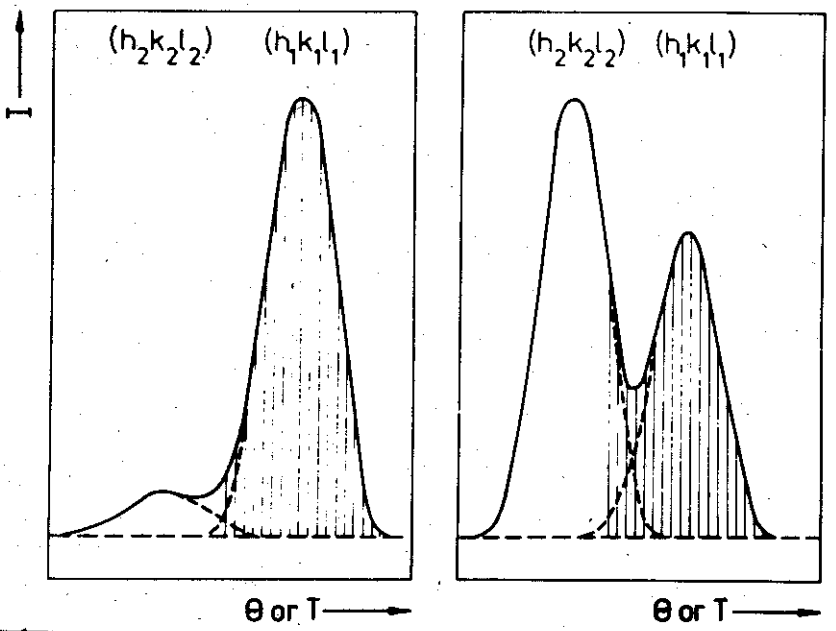

Figure 6

Intensity relation of two overlapped Bragg reflections (hkl) from a texturized sample at different specimen positions. The angle dispersive method records the shaded area. Using TOF technique the curve can be separated in two single peaks.

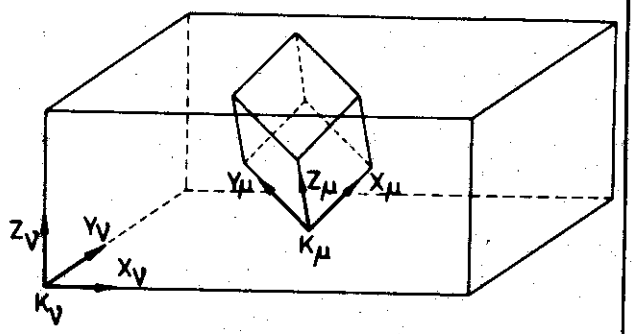

Figure 7

Representation of specimen coordinate system K with respect to the crystal coordinate system K.

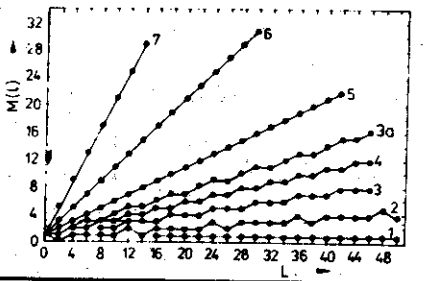

Figure 8

Number of linearly independent spherical harmonics in dependence on series expansion degree and symmetry for even l only 1-axial, 2-cubic, 3-hexagonal, 3a-trigonal, 4-tetragonal, 5-orthorhombic, 6-monoclinic and 7-triclinic symmetry.

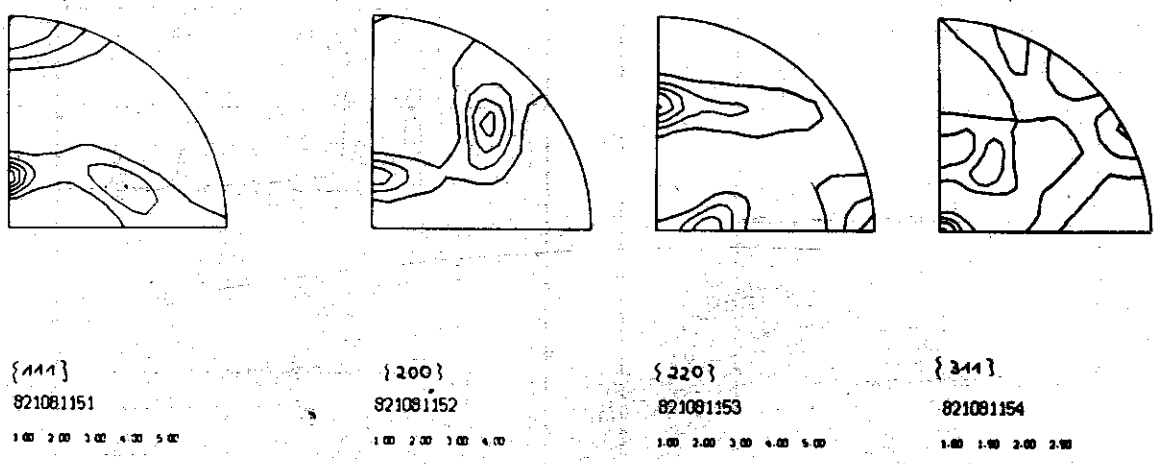

Figura 9a.

Experimental pole figures (111), (200), (220) and (311) for an Al-5Ca-5Zn alloy /45/.

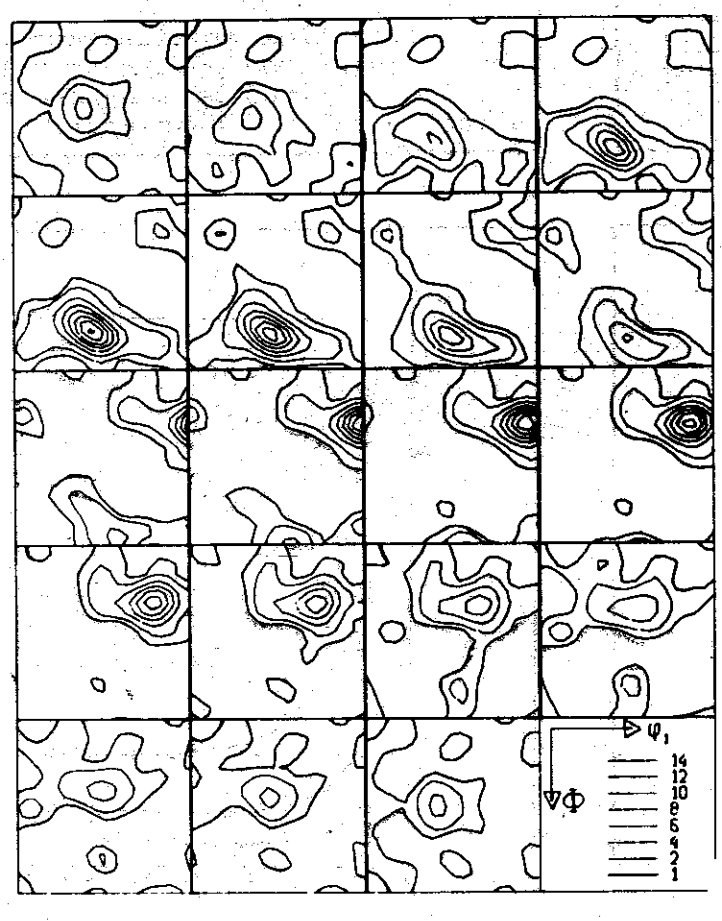

Figure 9b

ODF determined from pole figures of fig. 9a.

8210911

1.00 2.00 4.00 6.00 8.00 10.0 12.0 14.0

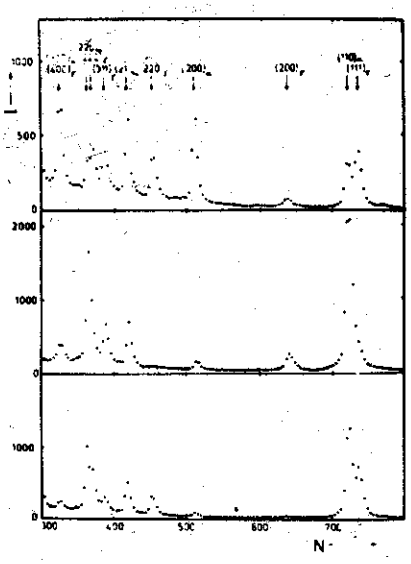

Figure 10

TOF diffraction pattern from a rolled sheet of microduplex steel for ND, RD and TD downward. I-intensity, N-number of time channel.

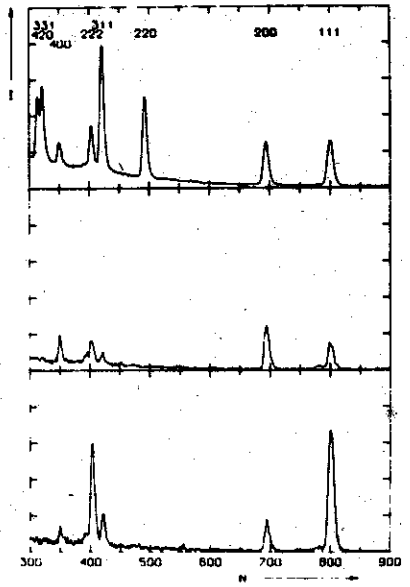

Figure 11

TOF diffraction spectra from copper for texture-free powder as well as for 96% deformed bars before and after annealing (downward).

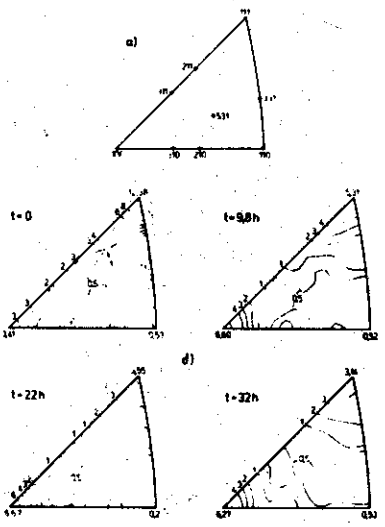

Figure 12

Inverse pole figures of copper bars for different annealing times at 225°C.

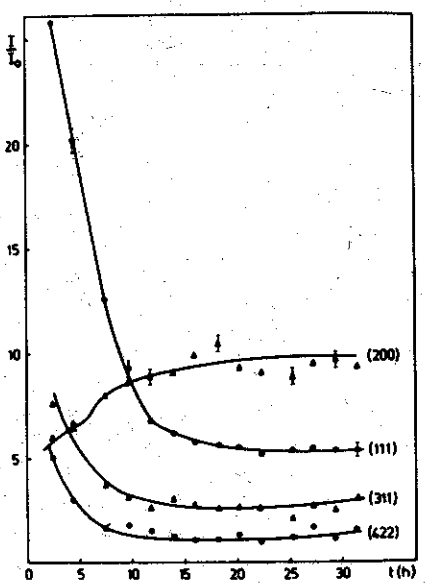

Figure 13

Intensity changes of Bragg reflections during recrystallization process.

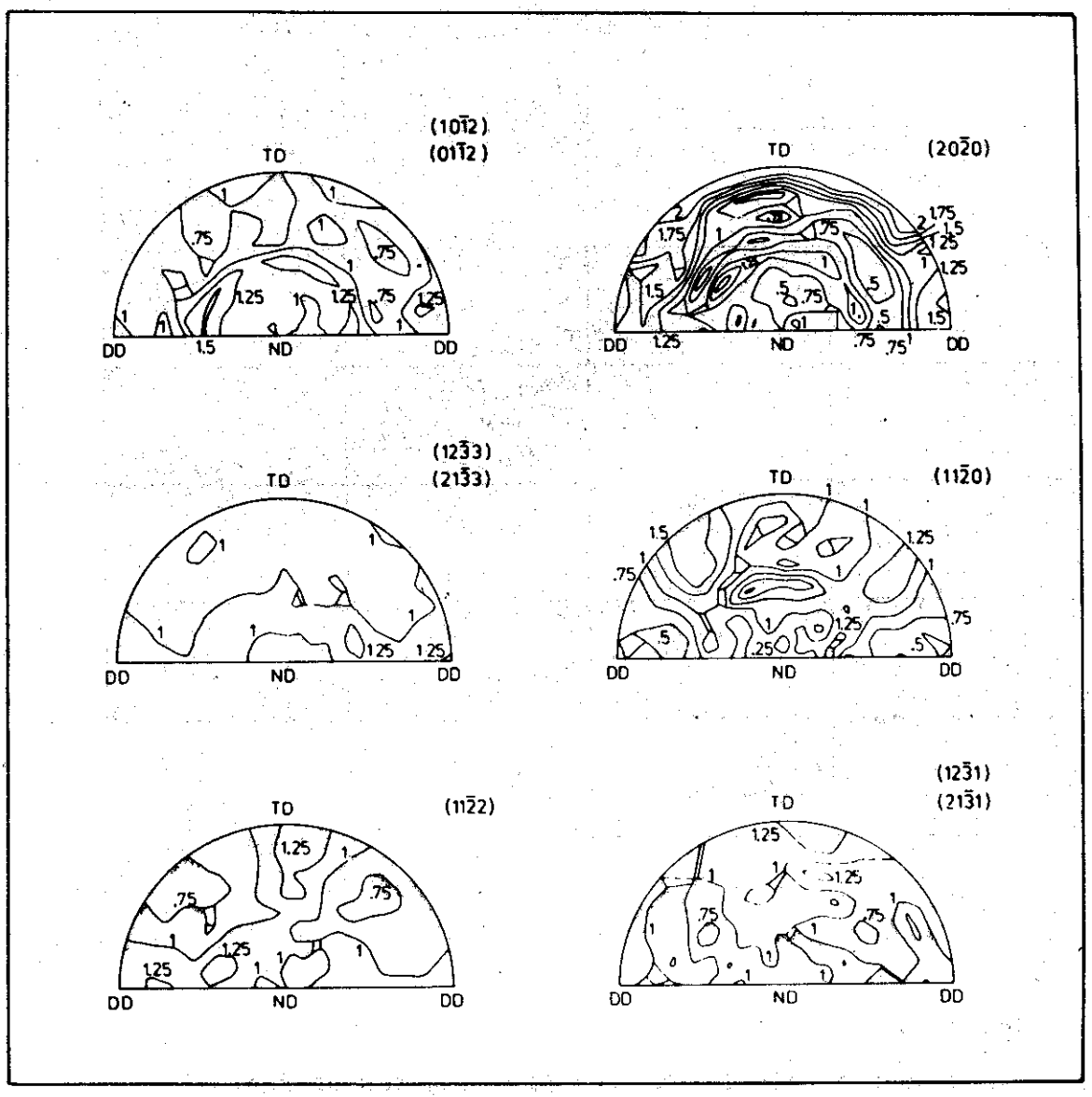

Figure 14

Pole figures of the quartz component in granulite.

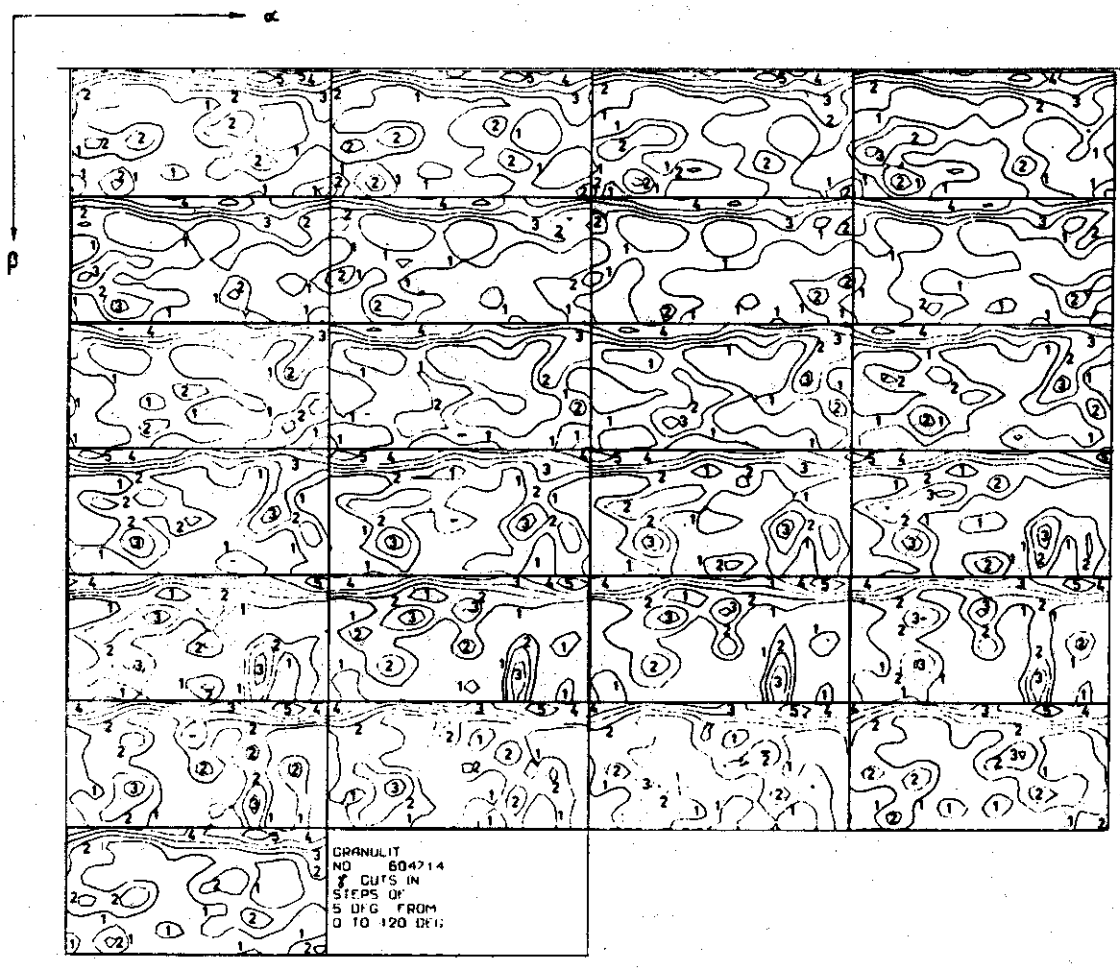

Figure 15

ODF of quartz calculated from pole figures of fig. 14.

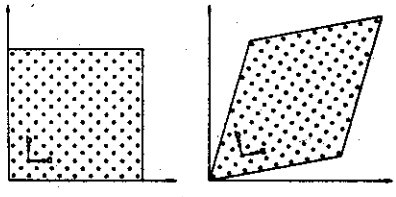

Figure 16

Plastic deformation of a crystallite in the Taylor model

a) before deformation the sample and crystal axes are parallel

b) to assimilate by gliding the imposed macroscopic deformation, the crystal axes are forced to rotate as shown.

REFERENCES

1. Lucke, K.; H.Perlwitz, W.Pitsch
   Phys. Stat. Sol. 7 (1964) 733.
2. Perlwitz, H.; K.Lucke; W.Pitsch
   Acta Met. 17 (1969) 1183.
3. Gerward, L.; S.Lehn; G.Christiansen,
   Texture 2 (1976) 95.
4. Matz, W.; K.Feldmann; M.Betzl; K.Henning; K.Walther; K.H.Kleinstuck, J.Tobisch, R.Sprungk
   Preprint CINR, ZfK-452, Rossendorf 1981.
5. Matthies, S.; K.Hennig
   Phys. Stat. Sol. (b) 113 (1982) 569.
6. Matthies, S.
   Kristall und Technik 15 (1980) 431.
7. Matthies, S.
   Kristall und Technik 15 (1980) 601.
8. Matthies, S.
   Kristall und Technik 15 (1980) 823.
9. Matthies, S.
   Kristall und Technik 15 (1980) 1189.
10. Matthies, S.
    Kristall und Technik 15 (1980) 1323.
11. Matthies, S.
    Crystal Research and Technology 16 (1981) 513.
12. Matthies, S.
    Crystal Research and Technology 16 (1981) 1061.
13. Matthies, S.
    Preprint CINR, ZfK-480, Rossendorf 1982.
14. Ruer, D.
    Thesis, Univ. Metz 1976.
15. Ruer, D.; R.Baro
    J.Appl. Crystallogr, 10 (1977) 458.
16. Imhof, I.
    Z.Metallkde 68 (1977) 38.
17. Imhof, I.
    Proc. of the 6th Int. Conf. on Textures of Materials, Tokyo 1981.

18. Roe, R.J.
J.Appl. Phys. 36 (1965) 2024.

19. Bunge, H.J.
Mathematische Methoden der Texturanalyse. Akademieverlag, Berlin 1969.

20. Bunge, H.J.
Texture Analysis of Materials, Mathematical Methods. Butterworth, London, Boston, Sydney, Wellington, Durban, Toronto 1982.

21. Jura, J.; J.Pospiech, Texture 3 (1978) 1.

22. Feldmann, K.
JINR Communication, P14-82-203, Dubna 1982.

23. Fichhorn, F.; A.Andreeff; M.Betzl; K.Walther; K.H.Kleinstuck, A.Mucklich; J.Tobisch; K.Feldmann; K.Hennig; D.Schlafer
JINR Communication, 18-12217, Dubna 1979.

24. Hennig, K.; K.Feldmann
Proc. of the IV School on Neutron Physics, Dubna 1982, p.358.

25. Klimanek, P.; A.Mucklich; K.Hennig
Proc. of the 6th Int. Conf. on Textures of Materials, Tokyo 1981.

26. Schreiter, K.; G.Hoetzsch; K.H.Kleinstuck; P.Klimanek; A.Mucklich, J.Tobisch; K.Hennig
Proc. of the 5th Int. Conf. on Textures of Materials, Springer, Berlin 1978.

27. Matz, W; K.Feldmann
JINR Communication, P14-82-265, Dubna 1982.

28. Morris, P.R.
J.Appl. Phys. 40 (1969) 447.

29. Nye, J.F.
Physical Properties of Crystals. Clarendon Press, Oxford 1957.

30. Matthies, S.
Phys. Stat. Sol.(b) 92 (1979) K135.

31. Wagner, F.; H.R.Wenk; C.Esling; H.J.Bunge
Phys. Stat. Sol.(a) 67 (1981) 261.

32. Bunge, H.J.; C. Esling
J.Phys. 40 (1979) L627.

33. Esling, C.; E.Bechler-Ferry; H.J.Bunge
J.Phys. 42 (1981) L141.

34. Virnich, K.H.; J.Pospiech; A.Flemmer; K.Lucke
Proc. of the 5th Int. Conf. on Textures of Materials, Springer,

Berlin 1978.

35. Feldmann, K.; L.Fuentes
JINR Preprint, E14-83-697, Dubna 1983.

36. Flemmer, A.
Thesis, RWTH Aachen 1976.

37. Matthies, S.; G.W.Vinel
Phys. Stat. Sol.(b) 112 (1982) K111

38. Matthies, S.; G.W.Vinel
Phys. Stat. Sol.(b) 112 (1982) K115.

39. Williams, R.O.
J.Appl. Phys. 39 (1968) 4329.

40. Taylor, G.L.
J.Inst. Metals 62 (1938) 307.

41. Bishop, J.F.W.
Phil. Mag. 44 (1953) 51.

42. Bishop, J.F.W.
R.Hill, Phil. Mag. 42 (1951) 414.

43. Chin, G.Y., W.L.Mammel
Trans. Met. Soc. AIME 245 (1969) 1211

44. Lister, G.S., M.S.Paterson, B.E.Hobbs
Tectonophysics 45 (1978) 107.

45. Novikov, I.I. et al.,
Proc. 4th Int. Symp. on Metallurgy and Material Science,
Riso 1983, p.467.

Recibido: 20 de enero de 1985.